energies

MDPI

Article

Secondary Frequency Stochastic Optimal Control in Independent Microgrids with Virtual Synchronous Generator-Controlled Energy Storage Systems

Ting Yang [1,*], Yajian Zhang [1], Zhaoxia Wang [2] and Haibo Pen [1]

[1] Key Laboratory of Smart Grid of Ministry of Education, Tianjin University, Nankai District, Tianjin 300072, China; zhang_ya_jian@tju.edu.cn (Y.Z.); penhaibo@tju.edu.cn (H.P.)
[2] Agency for Science, Technology and Research, Singapore 138632, Singapore; wangz@ihpc.a-star.edu.sg
* Correspondence: yangting@tju.edu.cn; Tel.: +86-1350-210-5487

Received: 8 August 2018; Accepted: 29 August 2018; Published: 11 September 2018

Abstract: With the increasing proportion of renewable energy in microgrids (MGs), its stochastic fluctuation of output power has posed challenges to system safety and operation, especially frequency stability. Virtual synchronous generator (VSG) technology, as one effective method, was used to smoothen frequency fluctuation and improve the system's dynamic performance, which can simulate the inertia and damping of the traditional synchronous generator. This study outlines the integration of VSG-controlled energy storage systems (ESSs) and traditional synchronous generators so they jointly participate in secondary frequency regulation in an independent MG. Firstly, a new uncertain state-space model for secondary frequency control is established, considering the measurement noises and modelling error. Then, an improved linear quadratic Gaussian (LQG) controller is designed based on stochastic optimal control theory, in which the dynamic performance index weighting matrices are optimized by combining loop transfer recovery (LTR) technology and the distribution estimation algorithm. On the issue of secondary frequency devices' output power allocation, the dynamic participation factors based on the ESS's current state of charge (SOC) are proposed to prevent the batteries' overcharging and overdischarging problems. The energy storage devices' service life can be prolonged and OPEX (operational expenditure) decreased. Multiple experimental scenarios with real parameters of MGs are employed to evaluate the performance of the proposed algorithm. The results show that, compared with the lead-compensated-proportional-integral-derivative (LC-PID) control and robust μ-control algorithms, the proposed stochastic optimal control method has a faster dynamic response and is more robust, and the fluctuations from renewable energy and power loads can be smoothened more effectively.

Keywords: secondary frequency control; independent microgrids (MGs); virtual synchronous generator (VSG); participation factors; linear quadratic Gaussian (LQG) control

1. Introduction

Energies such as photovoltaic (PV) and wind power are widely applied as the main sources for independent microgrids (MGs), since they enjoy advantages such as cleanliness and renewability [1–3]. However, the intermittent and stochastic active power output may have a detrimental effect on system frequency stability [4]. The reasons can be summarized as follows: (i) a mismatch between power load demand and power generation may be exacerbated by the superposition of the renewable/load fluctuation, which may lead to frequency deviation problems or even over-limit [5]; (ii) the application of large-scale renewables in independent MGs is equivalent to decreasing the proportion of traditional synchronous generators. However, conventional converters have almost no inertia support due to low output impedance, which reduces the reserve capacity to keep system

stability [6,7]. Hence, the frequency oscillation will be intensified when power mismatching occurs in independent MGs. Additionally, the flexible access/exit of renewable energy and loads may change the structure and the operating parameters of the MG system. All these difficulties have resulted in higher requirements of the robustness and dynamic performance of the frequency control system [8].

Generally, a hierarchical control approach (i.e., primary, secondary and tertiary control) is adopted in frequency regulation in independent MGs [9]. For primary control in MGs, the existing researches mainly focus on designing converter control strategies. Then the output power of ESSs can be adjusted with the frequency deviation. Droop control, as one of the representative control strategies, can reversely regulate the output power with frequency fluctuation via simulating drooping characteristic of synchronous generators [10,11]. However, it still has low inertia support for the MG and the amplitude of frequency deviation is still large when power mismatch occurs. Virtual synchronous generator (VSG) control technology, as a novel converter control method, has been proposed and applied to frequency regulation in an electrical power system. By simulating the swing equation and the excitation equation of the synchronous generator, the VSG converter calculates the control instructions of the ESSs' output voltage—including amplitude, frequency and phase—to participate in the frequency regulation. But most current research on VSG control only focuses on realizing the primary frequency or voltage regulation, i.e., the VSG adjusts its output to provide the power support in the independent MG's frequency or voltage regulation in real-time [12–14]. As we know, primary frequency control is a type of differential regulating method that cannot restore the frequency to the rated value. The frequency deviation will destroy the quality of the power supply. Hence, it is worth exploring new VSG control methods to realize the secondary frequency control.

In current research on secondary frequency control in independent MGs, decentralized and centralized models are the two main control structures. Liu et al. [15] have proposed a decentralized multi-agent control strategy to restore frequency to the rated value when there is a power mismatch. Unlike the decentralized model, Liu et al. [16] proposed a centralized secondary frequency control strategy. With a comparative analysis of the above two control models, Olivares et al. [17] pointed out that the centralized control structure was more suitable for independent MGs. Most researchers focus on the secondary frequency controller design. Kim et al. [18] presented a controller using ESSs and synchronous generators to compensate for the frequency deviation's high and low frequency components respectively. A lead-compensated-proportional-integral-derivative (LC-PID) controller was designed in the secondary control loop to restrain error and disturbance by the systems' stochastic noises. But the dynamic performance of a PID controller relies more on the established system model's accuracy. Moreover, the PID control algorithm depends on a precise system model which is hard to adapt to the system's operating point change from the renewable energy generators or power loads' change [19–21]. The actual system operation inevitably includes measurement noises, which will destroy the system's robustness and dynamic performance [22,23]. Based on μ-synthesis theory, Han et al. [24] proposed a secondary frequency controller using the D-K iteration algorithm to obtain the controller parameters. Robust H_∞ theory is also used to control the distributed generation system in MGs [25,26]. Furthermore, Bevrani et al. [27] analyzed the differences in control performance between the μ-synthesis and H_∞ control methods. However, to solve the uncertainty problem, most current robust controllers had to be designed conservatively, which weakened the dynamic performance, such as overshoot, settling time, steady-state time, etc. Fixed power allocation among generator units during frequency regulation processing may lead to storage battery overcharge or overdischarge, which will shorten the ESSs' service life.

To solve the above problems, in this paper, a stochastic optimal control method is proposed to realize secondary frequency regulation in independent MGs. The contributions are as follows:

(1) To solve the independent MG system uncertainty problem—resulting from the power fluctuation of renewables, load disturbance, and measurement noise—an uncertain state-space model for secondary frequency regulation with VSG-controlled ESSs and traditional synchronous generators is established. In the model, a participation factor dynamic configuration method for secondary frequency regulation

based on the battery's state of charge (SOC) is proposed to optimally control the ESSs, which will prevent the overcharge or overdischarge problems and prolong the ESSs' service life.

(2) According to the proposed uncertain state-space model for secondary frequency regulation in independent MGs, based on stochastic optimal control theory, an improved linear quadratic Gaussian (LQG) controller is designed to solve the established uncertain state-space model. In the controller design process, the weighting matrices determining the dynamic control performance are optimized by combining the loop transfer recovery (LTR) technology and distributed estimation algorithm. Compared with the PID and μ-synthesis control approaches, our proposed controller has a faster response speed and smaller overshoot, while the robustness is similar to the benchmark controllers.

The rest of this paper is organized as follows. Section 2 presents the independent MG structure, and establishes the uncertain state-space model of secondary frequency regulation. The participation factor dynamic configuration method based on the energy storage battery's SOC is also proposed in this section. With LTR technology, the improved LQG controller is designed in Section 3. In Section 4, the proposed controller's performance is evaluated based on a series of independent MG experimental scenarios. Concluding remarks are given in Section 5.

2. Frequency Regulation Modelling in Independent Microgrids

An independent MG usually contains the traditional synchronous generators (e.g., micro-gas turbine generator and diesel generators) and renewable energy generators (e.g., wind and PV power) as power supply units. The power load is usually comprised of conventional residential and industrial consumption, as well as novel variable consumptions (e.g., plug-in electrical vehicles). Besides the above, the system is also equipped with the appropriate ESSs (batteries, supercapacitors, flywheel, etc.) to stabilize the fluctuations from the renewables and loads. Figure 1 illustrates the proposed framework of frequency regulation in an independent MG in which the number of engaged synchronous generators and ESSs are m and n. All renewable energies and ESSs use the power electronic converters as interfaces to connect to the MG. Using the VSG technique in the converters, which simulates the swing equation of traditional synchronous generators, the ESSs can provide more inertia and damping to the MG. The stochastic optimal control method is proposed to implement secondary frequency regulation with the participation of traditional synchronous generators and VSG-controlled ESSs.

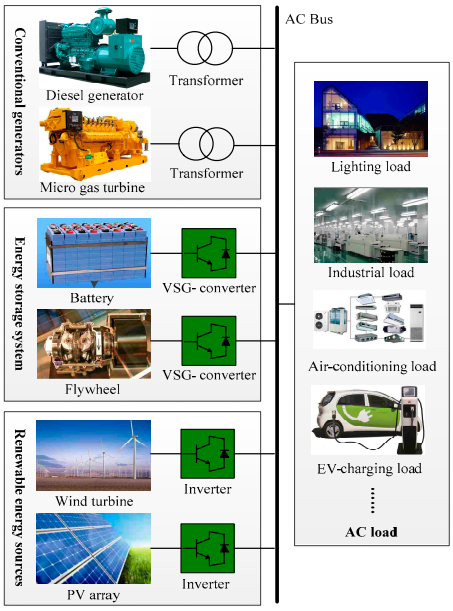

Figure 1. The control block diagram of an independent microgrid (MG).

2.1. State-Space Model for Secondary Frequency Regulation of Independent Microgrid

2.1.1. Traditional Synchronous Generator

A traditional synchronous generator consists of a governor, prime mover and synchronous generator to realize the secondary frequency regulating function. For the p-th traditional synchronous generator, simplified first order differential Equations (1)–(3) are used to describe the dynamic model [8]:

$$\frac{\mathrm{d}\Delta P_{\mathrm{v}1p}}{\mathrm{d}t} = -\frac{\Delta P_{\mathrm{v}1p}}{T_{\mathrm{G}1p}} + \frac{\Delta P_{1p}^{\mathrm{ref}}}{T_{\mathrm{G}1p}} - \frac{1}{T_{\mathrm{G}1p}R_{1p}}\Delta f \tag{1}$$

$$\frac{\mathrm{d}\Delta P_{\mathrm{m}1p}}{\mathrm{d}t} = -\frac{\Delta P_{\mathrm{m}1p}}{T_{\mathrm{T}1p}} + \frac{\Delta P_{\mathrm{v}1p}}{T_{\mathrm{T}1p}} \tag{2}$$

$$\frac{\mathrm{d}\Delta f}{\mathrm{d}t} = -\frac{D_{1p}}{M_{1p}}\Delta f - \frac{1}{M_{1p}}\Delta P_{\mathrm{d}} + \frac{1}{M_{1p}}\Delta P_{\mathrm{m}1p} \tag{3}$$

where $P_{\mathrm{v}1p}$ is the valve position of the governor, P_{1p}^{ref} is the commanded power value of the governor, $P_{\mathrm{m}1p}$ is the prime mover output power, R_{1p} is the droop coefficient, $T_{\mathrm{G}1p}$ and $T_{\mathrm{T}1p}$ are the time constants of the governor and turbine respectively, f is the MG frequency, M_{1p} and D_{1p} denote the inertia and damping of the traditional synchronous generator respectively, P_{d} is the power load of the MG, and the symbol "Δ" refers to the deviation from the rated value.

2.1.2. Virtual Synchronous Generator-Controlled Energy Storage System

The control principle diagram of a VSG-controlled ESS is shown in Figure 2. The SPWM module denotes that sine-wave pulse-width modulation technology is used to generate the drive instruction of the converter. For the q-th ESS, in order to simulate the inertia and damping of the traditional synchronous generators, the control algorithm employs the swing and droop equations as follows [12]:

$$\begin{cases} H_{2q}\frac{\mathrm{d}f}{\mathrm{d}t} = P_{\mathrm{in\_}2q}^{\mathrm{ESS}} - P_{\mathrm{out}} - D_{2q}(f_{\mathrm{VSG}} - f) \\ P_{\mathrm{in\_}2q}^{\mathrm{ESS}} = P_{2q}^{\mathrm{ref}} + P_{\mathrm{c\_}2q} = P_{2q}^{\mathrm{ref}} + \frac{1}{R_{2q}}(f - f_{\mathrm{VSG}}) \end{cases} \tag{4}$$

where H_{2q} is the virtual inertia, $P_{\mathrm{in\_}2q}^{\mathrm{ESS}}$ is the input power (i.e., the virtual prime mover power), D_{2q} is the damping coefficient, f_{VSG} is the frequency of the virtual rotor, P_{2q}^{ref} is the reference of active power of the ESS, $P_{\mathrm{c\_}2q}$ is the active power of the ESS for primary frequency regulation, and R_{2q} is the droop coefficient. $f_{\mathrm{VSG}} = f_{\mathrm{VSG}}^{*} + \Delta f$, $P_{\mathrm{in\_}2q}^{\mathrm{ESS}} = P_{\mathrm{in\_}2q}^{\mathrm{ESS}*} + \Delta P_{\mathrm{in\_}2q}^{\mathrm{ESS}}$, $P_{\mathrm{d}} = P_{\mathrm{d}}^{*} + \Delta P_{\mathrm{d}}$ and $P_{2q}^{\mathrm{ref}} = P_{2q}^{\mathrm{ref}*} + \Delta P_{2q}^{\mathrm{ref}}$, where superscript "*" and the symbol "Δ" refer to the static operating point and the corresponding deviation respectively. Therefore, in the system steady state, $P_{\mathrm{in\_}2q}^{\mathrm{ESS}*} = P_{2q}^{\mathrm{ref}*} = P_{\mathrm{out}}^{*}$ and $f_{\mathrm{VSG}}^{*} = f$, the small-signal model of VSG can be written as:

$$\begin{cases} H_{2q}\frac{\mathrm{d}\Delta f}{\mathrm{d}t} = \Delta P_{\mathrm{in\_}2q}^{\mathrm{ESS}} - \Delta P_{\mathrm{d}} - D_{2q}\Delta f \\ \Delta P_{\mathrm{in\_}2q}^{\mathrm{ESS}} = \Delta P_{2q}^{\mathrm{ref}} - \frac{1}{R_{2q}}\Delta f \end{cases} \tag{5}$$

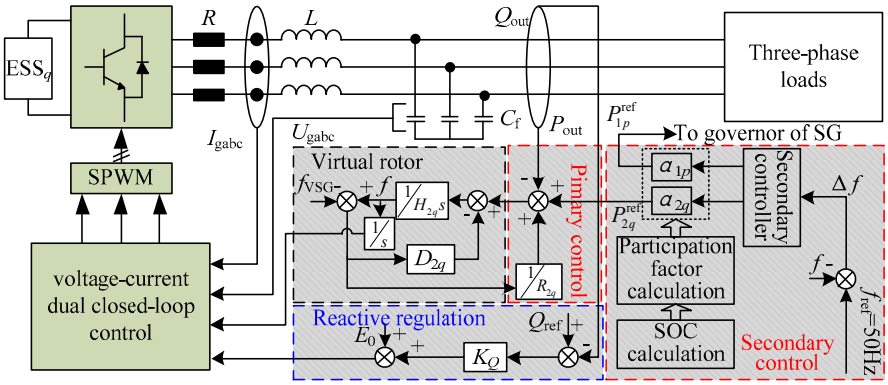

Figure 2. Block diagram of virtual synchronous generator (VSG).

2.1.3. Power Conservation Equation

The mismatch between the power load demand and generators' output power in an independent MG will lead to frequency deviation. Equation (6) expresses the relationship between the frequency deviation and the power mismatch:

$$(\sum_{p=1}^{m} M_{1p} + \sum_{q=1}^{n} H_{2q})\frac{d\Delta f}{dt} = -(\sum_{p=1}^{m} D_{1p} + \sum_{q=1}^{n} D_{2q})\Delta f + \Delta P_{PV} + \Delta P_W + \sum_{p=1}^{m} \Delta P_{m1p} + \sum_{q=1}^{n} \Delta P_{in\_2q}^{ESS} - \Delta P_d \quad (6)$$

where ΔP_{PV} and ΔP_W are the output power of PV and wind power units respectively.

2.1.4. Secondary Frequency Regulation Participation Factor Dynamic Configuration Method

In the current secondary frequency regulation approaches, the power allocation among the engaged devices is proportionally determined according to the power unit's rated adjustable capacities, not its current capacity. Hence, overcharge/overdischarge may occur in some energy storage batteries with unreasonable frequency regulation instruction, which will destroy the energy storage units' service life. To overcome this shortage, this paper proposes a dynamic participation factors adjusting strategy based on the ESS's current SOC. For the q-th ESSs, the SOC at time interval $[t_k, t]$ can be calculated as [28]:

$$SOC_q(t) = SOC_q(t_k) - \int_{t_k}^{t} \eta_q \Delta P_{2q}^{ref}(\tau)d\tau / E_{cq\_N} \quad (7)$$

where η_q is charging/discharging efficiency, which can be calculated as Equation (8), and E_{cq_N} is the rated capacity of ESS.

$$\eta_q = \begin{cases} 1/\eta, & \Delta P_{2q}^{ref} > 0 \\ \eta, & \Delta P_{2q}^{ref} < 0 \end{cases} \quad (8)$$

where η is the charge/discharge constant of the energy storage unit.

The power allocation among all engaged devices for secondary regulation is achieved through the participation factors. For a traditional synchronous generator, the output power for secondary frequency regulation is proportionally allocated according to its adjustable capacity. For VSG-controlled ESSs, the output power for secondary frequency regulation is corrected according to the current SOC value. The calculation formula of secondary frequency regulation factors is presented as:

$$\begin{cases} \alpha_{1p} = \frac{E_{1p}}{E_\Sigma} \\ \alpha_{2q} = \frac{E_{2q}}{E_\Sigma} - \frac{SOC_q(t) - SOC_{av}(t)}{SOC_\Sigma(t)}, P_{2q}^{ref} < 0 \\ \alpha_{2q} = \frac{E_{2q}}{E_\Sigma} + \frac{SOC_q(t) - SOC_{av}(t)}{SOC_\Sigma(t)}, P_{2q}^{ref} \geq 0 \end{cases} \quad (9)$$

where E_{1p} and E_{2q} are the adjustable capacities of the p-th traditional synchronous generator and the q-th VSG-controlled ESS respectively; $E_\Sigma = \Sigma_{p=1}^{m} E_{1p} + \Sigma_{q=1}^{n} E_{2q}$ is the total adjustable capacity of the

independent MG; $SOC_{\Sigma}(t)$ and $SOC_{av}(t)$ are the total SOC of all ESSs and the corresponding average value respectively.

2.2. Establishment of Uncertain State-Space Model of Secondary Frequency Regulation in Independent Microgrid

Based on the above analysis, the state-space model of secondary frequency regulation in an independent MG can be established. Unlike the current deterministic model, which inevitably includes the model errors, an uncertain state-space model of secondary frequency regulation is proposed in this paper. Let $\xi(t)$ and $\varepsilon(t)$ denote the model error and measurement error respectively. Without loss of generality, it is assumed that both $\xi(t)$ and $\varepsilon(t)$ are the independent *Gaussian* processes with zero means [8]. Their variances satisfy: $\mathrm{cov}[\xi, \xi] = r_1$, $\mathrm{cov}[\varepsilon, \varepsilon] = r_2$, $\mathrm{cov}[\xi, \varepsilon] = 0$. Accordingly, the uncertain state-space model of the secondary frequency regulation in independent MGs is proposed in Equation (10), in which $\boldsymbol{x} = [\Delta f, \Delta P_{\mathrm{m}11}, \ldots, \Delta P_{\mathrm{m}1m}, \Delta P_{\mathrm{v}11}, \ldots, \Delta P_{\mathrm{v}1m}]^{\mathrm{T}}$ denote the state vectors:

$$\begin{cases} \frac{\mathrm{d}}{\mathrm{d}t}\underbrace{\begin{bmatrix} \Delta f \\ \Delta P_{\mathrm{m}11} \\ \vdots \\ \Delta P_{\mathrm{m}1m} \\ \Delta P_{\mathrm{v}11} \\ \vdots \\ \Delta P_{\mathrm{v}1m} \end{bmatrix}}_{\boldsymbol{x}} = \underbrace{\begin{bmatrix} K_1 & \frac{1}{M_{\mathrm{eq}}} & \cdots & \frac{1}{M_{\mathrm{eq}}} & 0 & \cdots & 0 \\ 0 & -\frac{1}{T_{\mathrm{T}11}} & \cdots & 0 & \frac{1}{T_{\mathrm{T}11}} & \cdots & 0 \\ \vdots & \vdots & \ddots & \vdots & \vdots & \ddots & \vdots \\ 0 & 0 & \cdots & -\frac{1}{T_{\mathrm{T}1m}} & 0 & \cdots & \frac{1}{T_{\mathrm{T}1m}} \\ -\frac{1}{T_{\mathrm{G}11}R_{11}} & 0 & \cdots & 0 & -\frac{1}{T_{\mathrm{G}11}} & \cdots & 0 \\ \vdots & \vdots & \ddots & \vdots & \vdots & \ddots & \vdots \\ -\frac{1}{T_{\mathrm{G}1m}R_{1\mathrm{m}}} & 0 & \cdots & 0 & 0 & \cdots & -\frac{1}{T_{\mathrm{G}1m}} \end{bmatrix}}_{\mathbb{A}} \begin{bmatrix} \Delta f \\ \Delta P_{\mathrm{m}11} \\ \vdots \\ \Delta P_{\mathrm{m}1m} \\ \Delta P_{\mathrm{v}11} \\ \vdots \\ \Delta P_{\mathrm{v}1m} \end{bmatrix} + \underbrace{\begin{bmatrix} K_2 \\ 0 \\ \vdots \\ 0 \\ \frac{\alpha_{11}}{T_{\mathrm{G}11}} \\ \vdots \\ \frac{\alpha_{1m}}{T_{\mathrm{G}1m}} \end{bmatrix}}_{\mathbb{B}} u + \underbrace{\begin{bmatrix} \frac{1}{M_{\mathrm{eq}}} \\ 0 \\ \vdots \\ 0 \\ 0 \\ \vdots \\ 0 \end{bmatrix}}_{\mathbb{H}} (\Delta P_{\mathrm{PV}} + \Delta P_{\mathrm{W}} - \Delta P_{\mathrm{d}}) + \xi(t) \\ y(t) = \underbrace{\begin{bmatrix} 1 & 0 & \cdots & 0 & 0 & \cdots & 0 \end{bmatrix}}_{\mathbb{C}} \boldsymbol{x} + \varepsilon(t) \end{cases} \tag{10}$$

where $M_{\mathrm{eq}} = \sum_{p=1}^{m} M_{1p} + \sum_{q=1}^{n} H_{2q}$, $D_{\mathrm{eq}} = \sum_{p=1}^{m} D_{1p} + \sum_{q=1}^{n} D_{2q}$ denote the equivalent inertia and damping of MG respectively, $K_1 = -\frac{D_{\mathrm{eq}}}{M_{\mathrm{eq}}} - \frac{1}{M_{\mathrm{eq}}} \sum_{q=1}^{n} \frac{1}{R_{2q}}$, and $K_2 = \frac{1}{M_{\mathrm{eq}}} \sum_{q=1}^{n} \alpha_{2q}$. Figure 3 shows the control diagram.

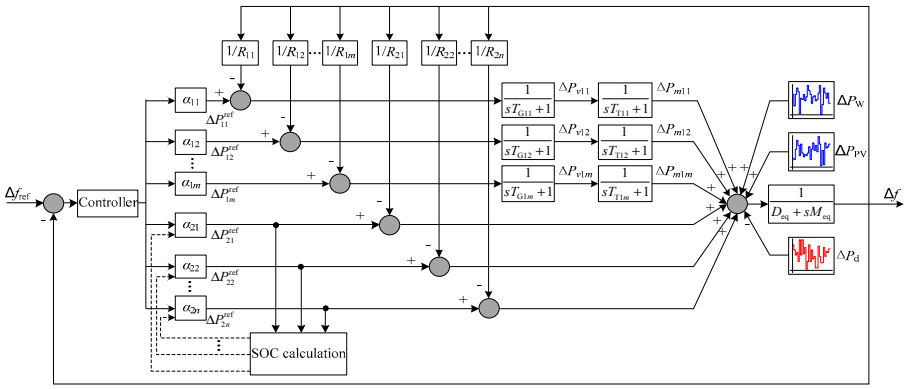

Figure 3. Control diagram of secondary frequency regulation in an independent MG.

3. Secondary Frequency Regulation Controller Design

This section details the experimental results, their interpretation and the experimental conclusions that can be drawn. To solve the proposed uncertain state-space model of secondary frequency regulation in independent MGs, a novel secondary controller is designed based on the LQG method with LTR technology.

The LQG control problem is to find the optimal control law $u(t)$ that can minimize the quadratic index Υ determined by the state vector and control input:

$$\Upsilon = E\left\{ \int_0^\infty \boldsymbol{x}^{\mathrm{T}}(t)\boldsymbol{Q_1}\boldsymbol{x}(t) + u^{\mathrm{T}}(t)\boldsymbol{Q_2}u(t)\mathrm{d}t \right\} \tag{11}$$

where $\boldsymbol{Q_1}$ and $\boldsymbol{Q_2}$ are weighting matrices and they should satisfy $\boldsymbol{Q_1^{\mathrm{T}}} = \boldsymbol{Q_1} \geq 0$ and $\boldsymbol{Q_2^{\mathrm{T}}} = \boldsymbol{Q_2} > 0$. Generally, $\boldsymbol{Q_1}$ and $\boldsymbol{Q_2}$ are chosen as the diagonal ones [29]. Based on the separation principle [30], the above control problem can be simplified into two separate sub-problems:

(1) Optimal state estimation problem based on *Kalman* filtering theory, i.e., determine observer gain matrix $\boldsymbol{L} = \boldsymbol{P}\mathbb{C}^{\mathrm{T}}r_2^{-1}$ where $\boldsymbol{P}$ can be solved by the *Riccati* in Equation (12). In the equation, $\Lambda = \mathbb{H}(r_{\mathrm{d}} + r_{\mathrm{PV}} + r_{\mathrm{W}})\mathbb{H}^{\mathbf{T}} + \boldsymbol{R_1}$, where r_{d}, r_{PV} and r_{W} represent the power fluctuation variances of load, PV and wind power units respectively:

$$\mathbb{A}\boldsymbol{P} + \boldsymbol{P}\mathbb{A}^{\mathrm{T}} + \boldsymbol{\Lambda} - \boldsymbol{P}\mathbb{C}^{\mathrm{T}}r_2{}^{-1}\mathbb{C}\boldsymbol{P} = 0 \tag{12}$$

(2) Determine the state-feedback matrix $\boldsymbol{K_f} = \boldsymbol{Q_2^{-1}}\mathbb{B}^{\mathrm{T}}\boldsymbol{S}$, where $\boldsymbol{S}$ is the solution of *Riccati* in Equation (13):

$$\mathbb{A}^{\mathrm{T}}\boldsymbol{S} + \boldsymbol{S}\mathbb{A} + \boldsymbol{Q_1} - \boldsymbol{S}\mathbb{B}\boldsymbol{Q_2^{-1}}\,\mathbb{B}^{\mathrm{T}}\boldsymbol{S} = 0 \tag{13}$$

But the above separated design method splits the relationship between observer and feedback controller. The essential reason is that, when the *Kalman* observer requires fast convergence of measurement noise, it reduces the system's stability margin, and even causes instability [30]. In this paper, to avoid the above disadvantage, LTR technology is adopted to recover the state-feedback loop gain at the controlled object input. Through constructing virtual noise to obtain the *Kalman* observation matrix, partial poles of the observer and partial zeroes of the controlled plant can be dynamically, mutually eliminated. This can ensure that the closed-loop system has a larger stability margin while the rest poles are far away from the origin to guarantee that the dynamic performance is not affected.

Design target loop. Firstly, choose appropriate $\boldsymbol{Q_1}$ and $\boldsymbol{Q_2}$, and calculate the state-feedback matrix $\boldsymbol{K_f}$ with Equation (13). The optimization goal is: The maximum singular value of transfer function $\boldsymbol{\Phi}(s) = \boldsymbol{K_f}(s\boldsymbol{I} - \mathbb{A})^{-1}$ is small enough (<<1) in the high-frequency area, whereas the minimum singular value is large enough (>>1) in the low-frequency area, which can reach the required robust and dynamic performance. In this paper, we present a distributed estimation algorithm to optimize the matrices $\boldsymbol{Q_1}$ and $\boldsymbol{Q_2}$, which is different from the traditional empirical valuation. In this optimization problem, the objective function is minimizing the peak time of frequency response, maximum frequency deviation and the time at which frequency response becomes steady. A uniform distribution model was used to ensure fairness during the feasible solutions selection. Then the global optimization was achieved by constantly renewing the probability distribution of the whole solution space.

Recover state-feedback loop gain to the target loop gain: Constructing virtual noise as $\boldsymbol{\Lambda'} = l\boldsymbol{\Lambda}$ (l is an incremental positive sequence, $l \to \infty$), *Kalman* observation matrix $\boldsymbol{L}$ can be calculated by Equation (12). The open-loop transfer function $\boldsymbol{\Phi_{sys}}(s) = -\boldsymbol{\Phi_{LQG}}(s)\boldsymbol{\Phi_{plant}}(s)$ will approximate the target transfer function $\boldsymbol{\Phi}(s)$, where $\boldsymbol{\Phi_{LQG}}(s)$ and $\boldsymbol{\Phi_{plant}}(s)$ are transfer functions of controlled plant and LQG optimal controller. They can be calculated by Equations (14) and (15):

$$\boldsymbol{\Phi_{LQG}}\,(s) = -\boldsymbol{K_f}(s\boldsymbol{I} - \mathbb{A} + \mathbb{B}\boldsymbol{K_f} + \boldsymbol{L}\mathbb{C})^{-1}\boldsymbol{L} \tag{14}$$

$$\boldsymbol{\Phi_{plant}} = -\mathbb{C}(s\boldsymbol{I} - \mathbb{A})^{-1}\mathbb{B} \tag{15}$$

The overall design process is given in Figure 4.

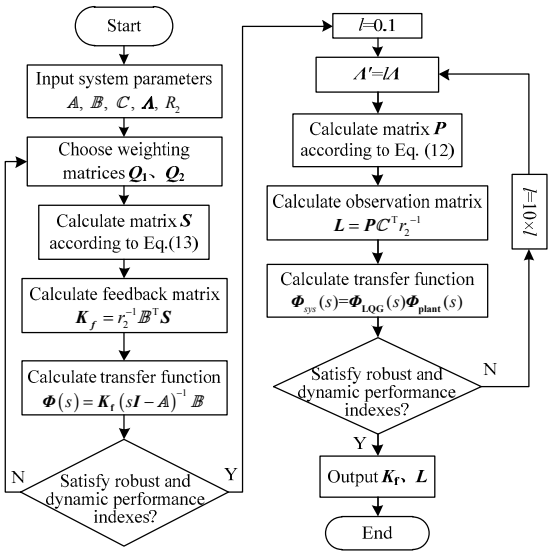

Figure 4. Flow chart of linear quadratic Gaussian (LQG)/loop transfer recover (LTR) controller design.

4. Experiment and Performance Evaluation

This section presents the details of the experiments conducted to evaluate the performance of our proposed control algorithm. The independent MG experimental platform is composed of one 150 kW diesel generator, one 120 kW micro-gas generator, one 50 kW wind power generator, one 30 kW PV system and two ESSs with the rated power as 50 kW and 30 kW. The system operating parameters of each unit come from a real system, as shown in Table 1.

Table 1. Parameters of a real microgrid system. SOC: state of charge.

Parameters of Traditional Synchronous Generators	**Diesel Generator**	**Micro-Gas Generator**
Time constant of speed governor T_G (s)	0.1	0.1
Time constant of generator T_T (s)	3	8
Droop coefficient R (Hz/pukW)	2.5	2.5
Rotary inertia M (pukW·s/Hz)	0.12	0.15
Damping coefficient D (pukW/Hz)	0.1	0.05
Adjustable power capacity E (kW·h)	110	85
Parameters of Renewable Generation Systems	**Wind Power Generator**	**PV System**
Baseline active output power	50	30
Variance of active output power fluctuation	15	10
Parameters of VSG-Controlled ESSs	**ESS1**	**ESS2**
Droop coefficient R (Hz/pukW)	2.5	2.05
Virtual rotary inertia (pukW·s/Hz)	0.2	0.17
Virtual damping coefficient (pukW/Hz)	0.19	0.22
Initial SOC value (%)	80	60
Constant η (%)	95	95
Rated active power P_N (kW)	50	30
Adjustable capacity E (kW·h)	36	20

The initial load power is 350 kW and the load fluctuation variance is 65 kW^2. The variance matrix of model error is $r_1 = 1 \times 10^{-3} I_{5\times5}$, and the variance of measurement noise is $r_2 = 1 \times 10^{-4}$. The secondary frequency controller is designed based on the proposed approach in this paper. We studied the robust and dynamic performance of our proposed control algorithm and compared it with the LC-PID control [18] and robust μ control [27] as benchmarks. The simulation schematic diagram is presented in Figure 5.

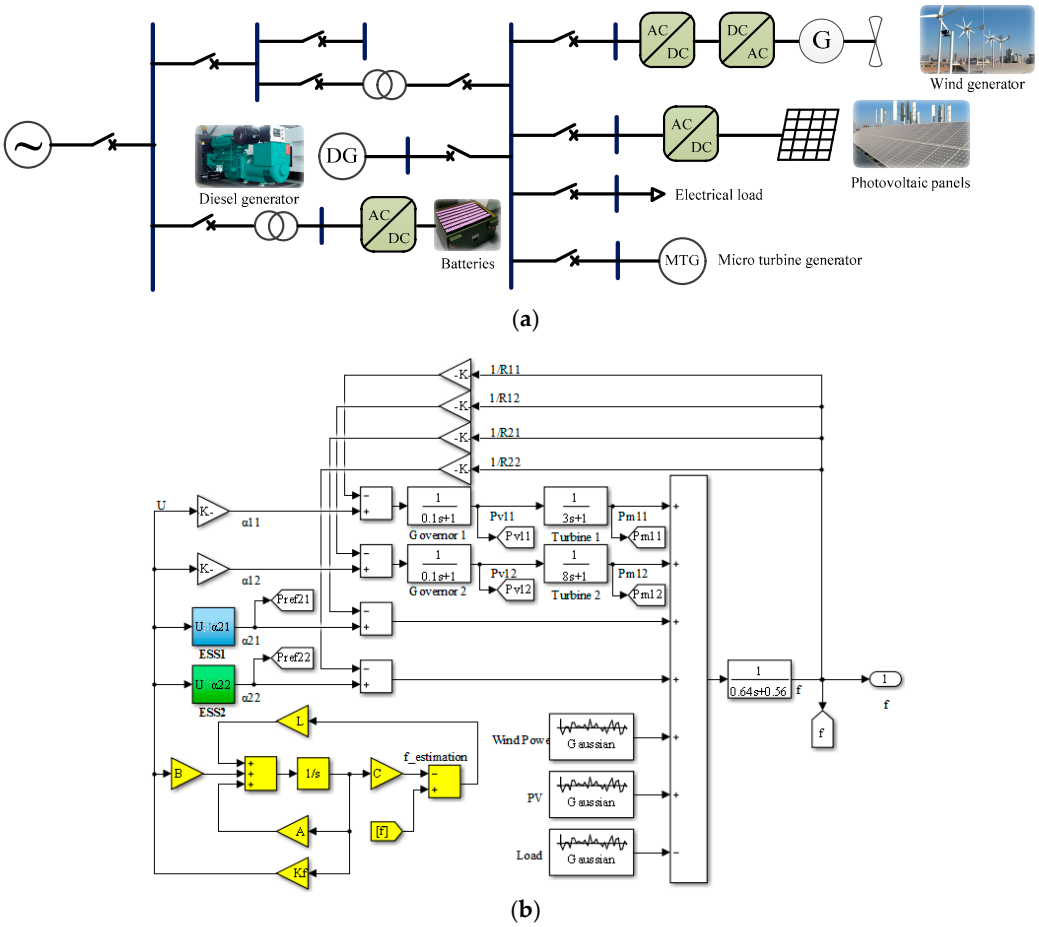

Figure 5. (**a**) The overall framework for frequency regulation in a real MG system; and (**b**) the simulation modular.

4.1. Dynamic Performance Analysis with Different Control Algorithms

First, the proposed control algorithm's performance in stabilizing the renewable energies and load fluctuation is evaluated. Let $\Delta P_{eq} = \Delta P_d - \Delta P_W - \Delta P_{PV}$ denote the equivalent power fluctuation value of renewable energies and loads, and the fluctuation curve of ΔP_{eq} at the short time interval [0, 50 s], as shown in Figure 6a. The corresponding frequency responses with different secondary frequency control algorithms are shown in Figure 6b. The maximum frequency deviations with LC-PID control, μ control and the proposed improved LQG control are 0.127 Hz, 0.022 Hz and 0.021 Hz respectively. It can be seen that the maximum frequency deviation with our proposed control method is decreased by 83.46% compared with the LC-PID control. The time values for reaching a steady state in the different cases are 6.06 s, 3.43 s and 2.14 s, respectively. Hence, the proposed control method has a better dynamic performance compared with the selected benchmarks, which can shorten the recovery time by 64.69% compared with the LC-PID controller, and by 37.61% compared with the robust μ controller. The reason is that the proposed control method used the distributed estimation algorithm to optimize the dynamic performance index weighting matrices. Conversely, the μ controller is designed by minimizing the H_∞ norm to guarantee the control performance in the worst situation, in which the controller is too conservative and the dynamic performance is poor, with a longer recovery time.

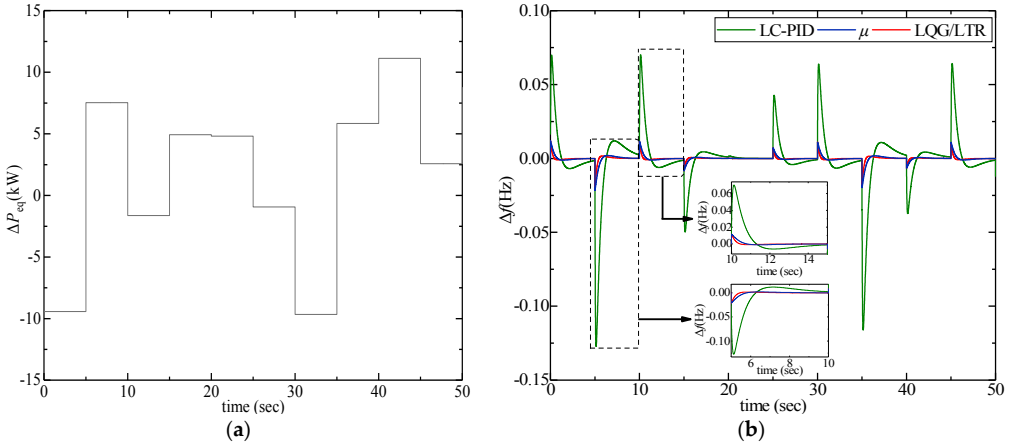

Figure 6. (**a**) The fluctuation curve of equivalent load ΔP_{eq}; and (**b**) dynamic frequency responses.

4.2. Performance Evaluation of Control Algorithms under Different Renewable and Load Power Fluctuations

Furthermore, the robust performance of the different renewable energies and load power fluctuations, shown in Table 2, is evaluated in this section. There are four scenarios: Scenarios 1 and 2 are the different fluctuations of wind and PV generators' output power, and Scenarios 3 and 4 are the different load fluctuations. Figure 7 shows the ΔP_{eq} fluctuation curves of the four scenarios. Frequency responses with different secondary frequency controllers in the four scenarios are presented in Figures 8 and 9. The results show that the LC-PID controller has a poorer performance with larger overshoot and slower response compared with the other two curves, showing that the LC-PID controller is less robust than the other two controllers. Further analyzing the performance of the μ controller and the proposed controller in the four scenarios, the improved LQG optimal controller also has better dynamic performance compared with the robust μ controller. The recovery times to reach the steady state can be shortened by 15.25%, 12.42%, 16.82% and 15.07% under the four scenarios, respectively.

Table 2. Uncertainties of load demand and renewable energy.

Variance	Scenario 1	Scenario 2	Scenario 3	Scenario 4
Wind power generator	+20%	−40%	-	-
PV generator	+45%	−30%	-	-
Power load	-	-	+50%	−40%

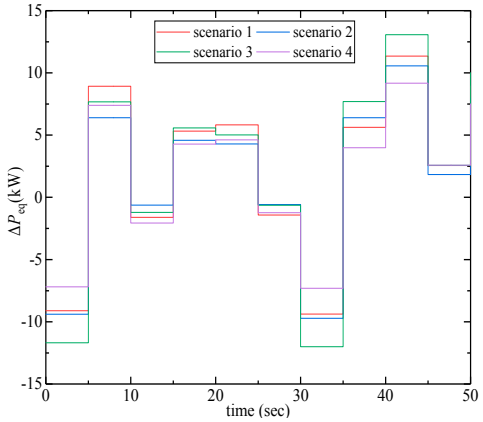

Figure 7. Fluctuations curves of ΔP_{eq} according to four scenarios.

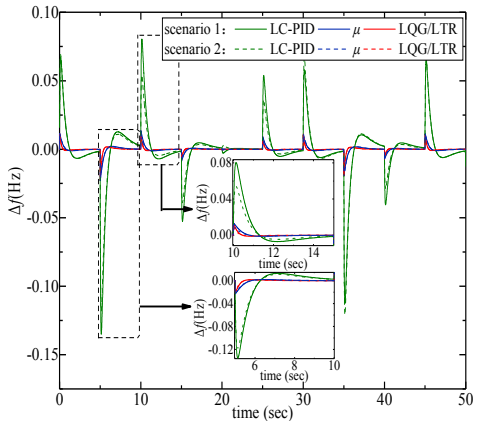

Figure 8. Frequency responses of MG according to renewable energy fluctuation of scenarios 1 and 2.

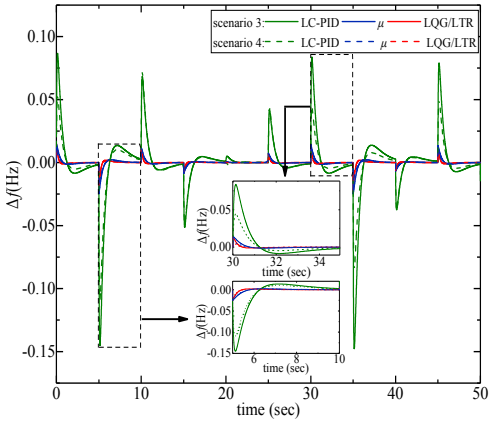

Figure 9. Frequency responses of MG according to power load fluctuation of scenarios 3 and 4.

4.3. Analysis of Energy Storage Units' Operating Status with Variable Participation Factors Strategy

In this section, we analyze the energy storage unit's improved operating performance following the variable participation factors strategy. The load fluctuation over an extended time period [0, 400 s] is shown in Figure 10a. Figure 10b illustrates the energy storage battery's SOC variation curves after adoption of the proposed variable participation factors strategy, compared with the conventional fixed participation factors strategy. The results show that since the current SOC values were not taken into consideration in the fixed participation factors, overdischarge occurs in ESS2 at the time intervals [86.7 s, 90 s], [148.8 s, 150 s] and [165.3 s, 175 s] (i.e., $SOC_2 \leq 0$), because the fixed participation factors strategy does not take into account the current SOC values. In this situation, ESS2 actually has no power supply capability for frequency regulation and the MG system cannot restore the frequency deviation to zero. On the other hand, the overdischarge also seriously damages the service life of the energy storage batteries. The proposed variable participation factors strategy can prevent the overcharge/overdischarge problem by considering the current SOC values of the energy storage batteries. During the entire experiment, the output power to support secondary frequency regulation was optimally allocated according to the current SOC values, and the overcharge/overdischarge problem could be avoided. Hence, the service life of ESSs can be prolonged and the OPEX reduced effectively.

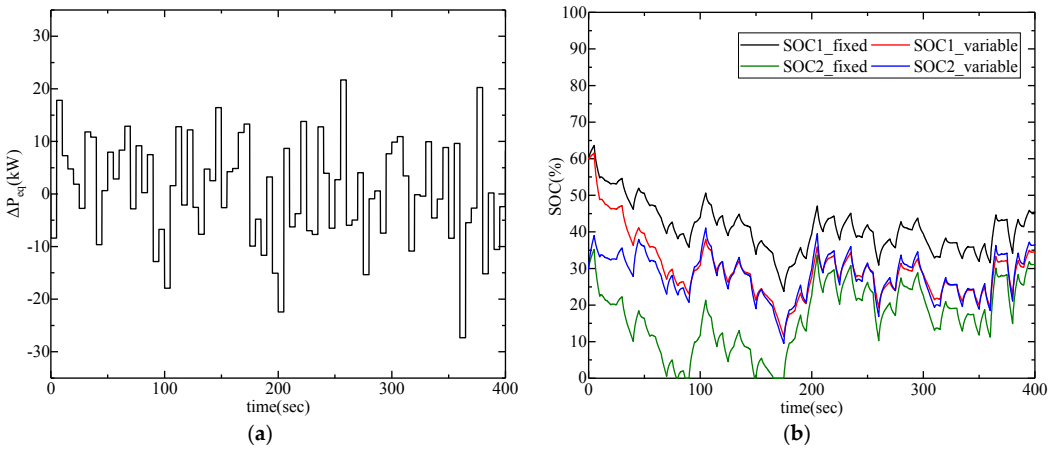

Figure 10. The SOC of ESSs with different participation factors strategy: (**a**) the fluctuation curve of equivalent load ΔP_{eq}; and (**b**) SOC values of the ESSs.

5. Conclusions

Frequency control in an independent MG is an effective way to ensure the stable operation and quality of the power supply. In this paper, a novel secondary frequency control strategy considering the participation of VSG-controlled ESSs in the independent MGs was proposed. Main conclusions were drawn as follows. (1) The frequency deviations caused by power mismatch (i.e., the fluctuations of loads and renewables) were effectively damped by the proposed secondary frequency control strategy. Compared with the LC-PID controller and the robust μ controller, the proposed control strategy had the faster response time, smaller variation and stronger robustness, which was potential to contribute to the frequency stability of the independent MGs; (2) The proposed variable participation factors calculation method, which took the SOC of engaged ESS into consideration, could adaptively adjust the output power to support the frequency regulation. Compared with the conventional fixed determination method, our proposed method could effectively avoid the overcharge and overdischarge and the service life could be correspondingly prolonged. Moreover, the system operation expenditure effectively can be reduced.

Author Contributions: Conceptualization, T.Y. and Y.Z.; Methodology, Y.Z.; Software, Y.Z.; Validation, T.Y. and Y.Z.; Formal Analysis, T.Y., Y.Z. and Z.W.; Investigation, Y.Z.; Resources, Z.W. and H.P.; Data Curation, T.Y. and Y.Z.; Writing-Original Draft Preparation, Y.Z.; Writing-Review & Editing, T.Y. and Z.W.; Visualization, H.P.; Supervision, T.Y. and Z.W.; Project Administration, T.Y. and Z.W.

Funding: This research was funded by the National Key Research and Development Program of China (2017YFB0903000); National Natural Science Foundation of China (61571324); Natural Science Foundation of Tianjin (16JCZDJC30900); National Program of International S&T Cooperation (2013DFA11040).

Conflicts of Interest: The authors declare no conflicts of interest.

References

1. Hosseinzadeh, M.; Salmasi, F. Robust optimal power management system for a hybrid AC/DC micro-grid. *IEEE Trans. Sustain. Energy* **2015**, *6*, 675–687. [CrossRef]
2. Fazio, A.; Russo, M.; Valeri, S.; Santis, M. Linear method for steady-state analysis of radial distribution systems. *Int. J. Electr. Power Energy Syst.* **2018**, *99*, 744–755. [CrossRef]
3. Swinand, G.P.; Omahoney, A. Estimating the impact of wind generation and wind forecast errors on energy prices and costs in Ireland. *Renew. Energy* **2015**, *75*, 468–473. [CrossRef]
4. Peng, C.; Xie, P.; Pan, L.; Yu, R. Flexible robust optimization dispatch for hybrid wind/photovoltaic/hydro/thermal power system. *IEEE Trans. Smart Grid* **2016**, *7*, 751–762. [CrossRef]
5. Vachirasricirikul, S.; Ngamroo, I. Robust LFC in a smart grid with wind power penetration by coordinated V2G control and frequency controller. *IEEE Trans. Smart Grid* **2014**, *5*, 371–380. [CrossRef]

6. Fini, M.H.; Golshan, M.E.H. Determining optimal virtual inertia and frequency control parameters to preserve the frequency stability in islanded microgrids with high penetration of renewables. *Electr. Power Syst. Res.* **2018**, *154*, 13–22. [CrossRef]
7. Zhou, X.; Chen, Y.; Zhou, L.; Luo, A.; Gueerrero, J.; Wu, W.; Yang, L.; Tan, W. Power coordinated control method with frequency support capability for hybrid single/three-phase microgrid. *IET Gener. Transm. Distrib.* **2018**, *12*, 2397–2405. [CrossRef]
8. Mohamed, T.H.; Morel, J.; Bevrani, H.; Hiyama, T. Model predictive based load frequency control design concerning wind turbines. *Int. J. Electr. Power Energy Syst.* **2012**, *43*, 859–867. [CrossRef]
9. Rezaei, N.; Kalantar, M. Economic–environmental hierarchical frequency management of a droop-controlled islanded microgrid. *Energy Convers. Manag.* **2014**, *88*, 498–515. [CrossRef]
10. Hosseinzadeh, M.; Salmasi, F. Fault-tolerant supervisor controller for a hybrid AC/DC micro-grid. *IEEE Trans. Smart Grid* **2018**, *9*, 2809–2823. [CrossRef]
11. Lai, J.; Zhou, H.; Lu, X.; Yu, X.; Hu, W. Droop-based distributed cooperative control for microgrids with time-varying delays. *IEEE Trans. Smart Grid* **2016**, *7*, 1775–1789. [CrossRef]
12. Fathi, A.; Shafiee, Q.; Bevrani, H. Robust frequency control of microgrids using an extended virtual synchronous generator. *IEEE Trans. Power Syst.* **2018**. [CrossRef]
13. Liu, J.; Miura, Y.; Bevrani, H.; Ise, T. Enhanced virtual synchronous generator control for parallel inverters in microgrids. *IEEE Trans. Smart Grid* **2016**, *8*, 2268–2277. [CrossRef]
14. Ma, Y.; Cao, W.; Yang, L.; Wang, F.; Tolbert, L.M. Virtual synchronous generator control of full converter wind turbines with short term energy storage. *IEEE Trans. Ind. Electron.* **2017**, *64*, 8821–8831. [CrossRef]
15. Liu, W.; Gu, W.; Sheng, W.; Meng, X.; Wu, Z.; Chen, W. Decentralized multi-agent system-based cooperative frequency control for autonomous microgrids with communication constraints. *IEEE Trans. Sustain. Energy* **2017**, *5*, 446–456. [CrossRef]
16. Liu, S.; Wang, X.; Liu, P.X. Impact of communication delays on secondary frequency control in an islanded microgrid. *IEEE Trans. Ind. Electron.* **2015**, *62*, 2021–2031. [CrossRef]
17. Olivares, D.E.; Mehrizi-Sani, A.; Etemadi, A.H.; Canizares, C.A.; Iravani, R.; Kazerani, M.; Hajimiragha, A.H.; Gomis-Bellmunt, O.; Saeedifard, M.; Palma-Behnke, R.; et al. Trends in microgrid control. *IEEE Trans. Smart Grid* **2014**, *5*, 1905–1919. [CrossRef]
18. Kim, Y.J.; Del-Rosario-Calaf, G.; Norford, L.K. Analysis and experimental implementation of grid frequency regulation using behind-the-meter batteries compensating for fast load demand variations. *IEEE Trans. Power Syst.* **2017**, *32*, 484–498. [CrossRef]
19. Mi, Y.; Fu, Y.; Li, D.; Wang, C.; Loh, P.C.; Wang, P. The sliding mode load frequency control for hybrid power system based on disturbance observer. *Int. J. Electr. Power Energy Syst.* **2016**, *74*, 446–452. [CrossRef]
20. Khooban, M.H.; Niknam, T.; Blaabjerg, F.; Davari, P.; Dragicevic, T. A robust adaptive load frequency control for micro-grids. *ISA Trans.* **2016**, *65*, 220–229. [CrossRef] [PubMed]
21. Vrdoljak, K.; Perić, N.; Petrović, I. Sliding mode based load-frequency control in power systems. *Electr. Power Syst. Res.* **2010**, *80*, 514–527. [CrossRef]
22. Vachirasricirikul, S.; Ngamroo, I. Robust controller design of heat pump and plug-in hybrid electric vehicle for frequency control in a smart microgrid based on specified-structure mixed H_2/H_∞ control technique. *Appl. Energy* **2011**, *88*, 3860–3868. [CrossRef]
23. Cai, L.; He, Z.; Hu, H. A new load frequency control method of multi-area power system via the viewpoints of Port-Hamiltonian system and cascade system. *IEEE Trans. Power Syst.* **2017**, *32*, 1689–1700. [CrossRef]
24. Han, Y.; Young, P.M.; Jain, A.; Zimmerle, D. Robust control for microgrid frequency deviation reduction with attached storage system. *IEEE Trans. Smart Grid* **2015**, *6*, 557–565. [CrossRef]
25. Babazadeh, M.; Karimi, H.; Babazadeh, M.; Karimi, H. A robust two-degree-of-freedom control strategy for an islanded microgrid. *IEEE Trans. Power Deliv.* **2013**, *28*, 1339–1347. [CrossRef]
26. Hossain, M.J.; Pota, H.R.; Mahmud, M.A.; Aldeen, M. Robust control for power sharing in microgrids with low-inertia wind and PV generators. *IEEE Trans. Sustain. Energy* **2015**, *6*, 1067–1077. [CrossRef]
27. Bevrani, H.; Feizi, M.R.; Ataee, S. Robust frequency control in an islanded microgrid: H_∞ and μ-synthesis approaches. *IEEE Trans. Smart Grid* **2016**, *7*, 706–717. [CrossRef]
28. Şerban, I.; Marinescu, C. Aggregate load-frequency control of a wind-hydro autonomous microgrid. *Renew. Energy* **2011**, *36*, 3345–3354. [CrossRef]

29. Zolotas, A.C.; Chaudhuri, B.; Jaimoukha, I.M.; Korba, P. A study on LQG/LTR control for damping inter-area oscillations in power systems. *IEEE Trans. Contr. Syst. Technol.* **2006**, *15*, 151–160. [CrossRef]
30. Angélico, B.A.; Toriumi, F.Y.; Barbosa, F.S.; Neves, G.D. On guaranteeing convergence of discrete LQG/LTR when augmenting it with forward PI controllers. *IEEE Access* **2017**, *5*, 27203–27210. [CrossRef]